

High-Resolution Imaging of Single Fluorescent Molecules with the Optical Near-Field of a Metal Tip

Heinrich G. Frey, Susanne Witt, Karin Felderer, and Reinhard Guckenberger*

Max-Planck-Institut für Biochemie, Abteilung Molekulare Strukturbiologie, Am Klopferspitz 18, 82152 Martinsried, Germany

(Received 15 January 2004; published 10 November 2004)

We show that a concentration of light at a metal tip allows near-field optical imaging of single fluorescent dye molecules at very high resolution, despite strong quenching effects. Details as small as 10 nm were observed in the fluorescence patterns of single Cy-3 dyes bound to the termini of DNA. Data evaluation by model fitting determines the positions of the dyes to an accuracy even better than 1 nm and also yields their 3D orientation. The metal tip simultaneously provides high-resolution topographic imaging complementing the optical signal for a detailed surface examination.

DOI: 10.1103/PhysRevLett.93.200801

PACS numbers: 07.79.Fc, 33.50.-j, 42.25.Gy, 87.64.Xx

Within the various kinds of optical microscopes, scanning near-field optical microscopes (SNOMs) [1] achieve the highest resolution since they do not suffer from diffraction effects. They take advantage of the high localization of optical fields at surfaces, localized at a length scale much smaller than the wavelength. SNOMs exploit these near-fields by scanning an optical probe of subwavelength size relative to the sample at a distance of a few nanometers. The optical resolution achievable is mainly limited by the size of the probe. The gap between the probe and sample is controlled by measuring force interactions, similar to the methodology of atomic force microscopes (AFMs). Thus, a SNOM provides simultaneously optical and topographical images of the sample surface.

Fluorescence is a widely used tool to identify structures in inhomogeneous samples, especially in biology. Of particular interest is the investigation of self-fluorescing or fluorescence labeled macromolecules at the single molecule level. However, it turned out to be very difficult to combine in a SNOM high optical and topographical resolution with single fluorophore sensitivity. In this Letter we report on a solution to this problem. We present highly resolved optical imaging of single dyes, complemented by high-resolution topographs, and describe how this imaging can be modeled. The excellent results became possible using a special SNOM probe that combines the respective advantages of the two main current kinds of SNOMs, the aperture and the scattering SNOM.

In fluorescence applications, a SNOM probe is operated as a very small light source and the locally excited fluorescence is measured. The aperture SNOM uses a subwavelength aperture for the light confinement. Detection of single molecule fluorescence is possible [2,3]. Resolution typically reaches a value of about 50 to 100 nm. In only a few cases higher resolution has been reported [4–6]. The scattering SNOM [7] (also called apertureless SNOM) is based upon the interaction of the optical near-field of a sharp metal or dielectric tip with the sample. Light is provided by a laser beam focused

onto the tip. As the light is concentrated at the apex of the sharp tip, this kind of SNOM achieves a very high resolution, routinely in the range of 10 to 20 nm [8]. Nevertheless, in fluorescence applications, a relatively large area of the sample around the tip is exposed to the laser light, resulting in a high background signal and the bleaching of dyes. Thus imaging of single fluorophores by scattering SNOM had quite limited success, although various attempts have been made [9–14], also with 2-photon excitation [15].

The new kind of SNOM probe, the “tip-on-aperture” (TOA) probe [16] used in our experiments comprises features of both types of SNOM, by illuminating a metal tip through a contiguous aperture as depicted in Fig. 1. The tip may be viewed as a support structure for surface plasmons. These plasmons will be excited at the base region of the tip by the aperture’s near-field (which is modified by the presence of the metal tip). They will propagate along the tip and be reflected back at the apex leading to standing waves. The plasmon fields are envisaged to concentrate at the apex in a fashion analogous to the lightning rod effect of electrostatics. In contrast to the aperture SNOM with its broad probe, both optical and topographical images taken with the TOA probe originate

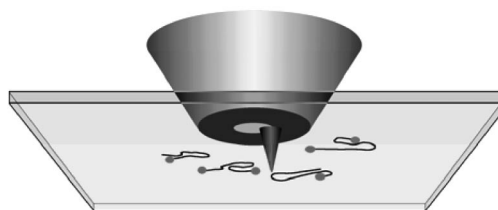


FIG. 1. Schematic drawing of the TOA probe with the DNA sample. The TOA probe consists of a sharp metal tip mounted on a conventional aperture probe. The aperture probe is made up of a tapered glass fiber coated laterally with metal, which confines the light to the glass except at the aperture in the front end. The sample consists of DNA with covalently bound Cy-3 molecules, prepared on mica.

from the identical part of the probe, the apex of the metal tip. Consequently, the simultaneously recorded optical and topographical images have a similar resolution and are, in good approximation, not shifted against each other.

The preparation of the TOA probe on a glass fiber is described in Ref. [16]. The metal tips are about 150 nm long, consist of Al, and are located at the aperture rim. The light from an argon laser ($\lambda = 514$ nm for our experiments) is coupled into the glass fiber illuminating the sample through such a TOA probe. Fluorescence light transmitted through the transparent sample is collected by a 0.95 numerical aperture objective of an inverse light microscope, filtered by a 550 nm long pass filter, and detected by an avalanche photodiode. Because of the asymmetry in the tip-aperture geometry, we have to adjust the polarization of the light coupled into the glass fiber for the best signal to background ratio [16]. About 1/3 of our probes provide good fluorescence results at such optimal polarization. The sample is scanned below the probe at a constant distance under shear force control at scan speeds in the range of 1 $\mu\text{m/s}$.

As samples we used Cy-3 fluorophores covalently bound to the termini of DNA. These samples were prepared in a standard polymerase chain reaction (PCR) by amplifying an approximately 1000 base pairs DNA molecule using vector DNA as the template and vector specific forward and reverse primer, which were 5'-end Cy-3 labeled (IBA). The PCR product was purified according to standard methods. Mica sheets were pretreated by applying 20 μl of a 400 mM NiCl_2 solution in water. After 2 min the solution was blotted off and a 30 μl drop of Cy-3 labeled DNA solution was applied. After 10 min the sample was washed with ultrapure water and blown dry by nitrogen.

Figure 2 shows a typical fluorescence image of such a specimen taken with our TOA probe. Most striking is the appearance of two-lobed patterns with distances between the maxima below 30 nm and a full width at half maximum (FWHM) of about 10 nm for each peak. As such patterns are found in all possible orientations, the shape of the patterns cannot be caused by a special shape of the probing tip (e.g., a double tip). The patterns belong to single fluorophores as indicated by the complete bleaching of some dyes between one scan line and the next one.

The observed image patterns of single dyes can be explained in analogy to patterns found with aperture SNOMs [2,3]. Single dyes monitor the field distribution of the probe. Vice versa, with a known field distribution, the orientation of a dye can be determined from a measured intensity pattern [2,3,17,18]. Our fluorescence patterns can be evaluated on the basis of a model commonly used in scattering SNOM [8,12,19]. The optical field of the probe below the tip is approximated by that of a point dipole, which is oriented along the tip axis and positioned in the center of a sphere fitted to the tip apex (Fig. 3). The dye molecules are also considered as dipoles, the excita-

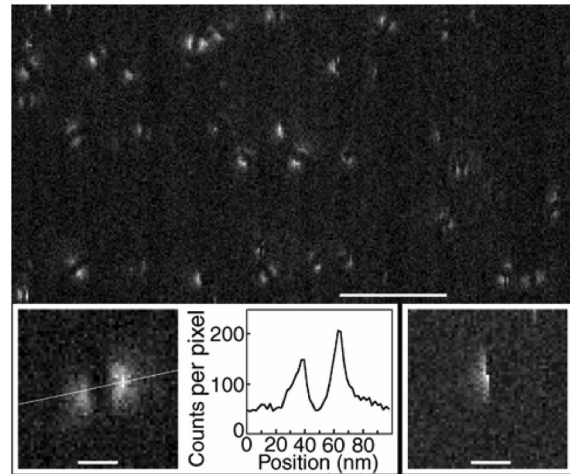


FIG. 2. Fluorescence image of single Cy-3 dye molecules, which appear mostly as double maxima. Scale bar: 200 nm. The inset on the left shows a zoomed image of a dye molecule together with a section along the line (three lines average). The maximum on the right has a value of only 10 nm for the FWHM. A bleaching event from one scan line (oriented vertically) to the next one is displayed enlarged in the inset on the right side. Scale bars for the insets: 25 nm.

tion of which is proportional to the squared field component parallel to their dipole moment. The residual field of the aperture itself at the sample is negligible in our setup. It is smaller than the field of the tip apex by a factor of at least 10, as concluded from images of fluorescent beads showing sharp bright spots within wide faint spots indicating the apex and the aperture field, respectively (data not shown).

According to the above model, a dye dipole oriented in the sample plane displays two symmetric maxima. The line connecting the maxima gives the dipole orientation in the plane (azimuth angle). Inclined dyes will give asymmetric peaks. A dye with a vertical orientation of its dipole experiences strongest excitation at a position directly below the tip. However, quenching by the metal tip affects the fluorescence. For vertically oriented dye dipoles maximal excitation coincides with the shortest

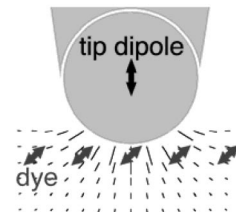


FIG. 3. Field below the TOA tip approximated by a dipole field. The strength and direction of the field is indicated by the length and orientation of the short lines. The excitation of a dye molecule is proportional to the squared field component parallel to the dye's absorption dipole moment. It depends strongly on orientation and position of the dye relative to the tip.

tip-dye distance. As a result, a vertical dye dipole will not give a single peak but a circular structure; for small tip-sample distances the dye is nearly completely quenched below the tip.

The imaging process of single fluorophores by our TOA probe was simulated using the software package MATHLAB 6.5 (Mathworks). Quenching corresponds to a reduction in lifetime, which was calculated with the classical expression given by Eq. (8) in Ref. [20]. In all our field calculations, first order mirror dipoles in the mica and the metal sphere, respectively, were taken into account with ϵ values $-44.7 + 15.0 i$ for Al and 2.56 for mica. The retroaction of the dye dipole on the tip dipole were neglected as well as retardation effects. To calculate the final signal, emission was considered only in directions, which are collected by the objective. Within this simulation program the following fit parameters were used. For each pattern separately: x, y position of the dye, its 3D orientation, a normalization factor for its brightness, and a local background; fit parameters assumed to be constant over the whole image: tip radius and tip height above the sample. For the quantum efficiency of a free molecule a value of 0.3 was taken.

Figure 4 shows the consistency of the experimental results with the modeled fluorescent patterns fitted to the data. The calculated parameters for the tip radius from Figs. 2 and 5 (12 nm) and Fig. 4 (22 nm) compare well with the typical tip radii between 15 and 25 nm measured by transmission electron microscopy. However, the calculated tip-sample distances of about 1 nm are lower than expected for a distance control by shear force. From approach curves we measured a distance between the probe and the sample of 2 to 3 nm, at oscillation amplitudes below 2 nm. Two effects will reduce the distance value calculated in the fits: (i) The conventional treatment [20] of the quenching effect neglects contributions with a stronger dependence on distance becoming important at distances below 5 nm [21]. (ii) The tip apex may be flattened in comparison to a sphere.

Our model explains the moonlike and ringlike patterns by strong quenching effects at tip-dye distances below about 3 nm. At a larger distance such patterns should turn

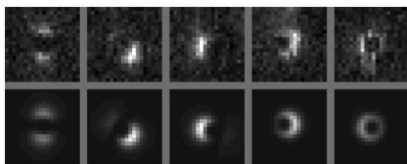


FIG. 4. Fluorescence patterns of differently tilted dye molecules. Upper row: Measurements (scan lines are oriented vertically, also in Figs. 5 and 6). Lower row: Patterns calculated with parameters fitted to the measurements. Resulting tilt angles out of the sample plane are 0° , 14° , 20° , 49° , and 68° . Fitted tip radius: 22 nm. Image sizes: 117 nm. The patterns are broader than in Figs. 2, 5, and 6 due to a blunter tip.

into single peaks. Correspondingly, we have never seen moons or rings with single dyes (Dil-C₁₈) embedded in poly(methyl methacrylate). For the two-lobed patterns in our DNA sample, the central minimum became smaller when increasing the tip-sample distance. At the same time, the total number of photon counts per pattern decreased, typically by a factor of 2 for an increase in distance of 5 nm, indicating predominance of near-field concentration. Quenching seems to be dominant only at very small distances, probably because of the small lateral size of the very end of our tip. This contrasts the more common situation with flat metal surfaces where quenching is effective over more than 10 nm distance. Besides quenching, redirection of the fluorescence light by the tip itself as in Ref. [22] may affect the shape of the observed fluorescence patterns. However, we have seen no indication of such effects in experiments with fluorescent beads of about 5 nm diameter [16].

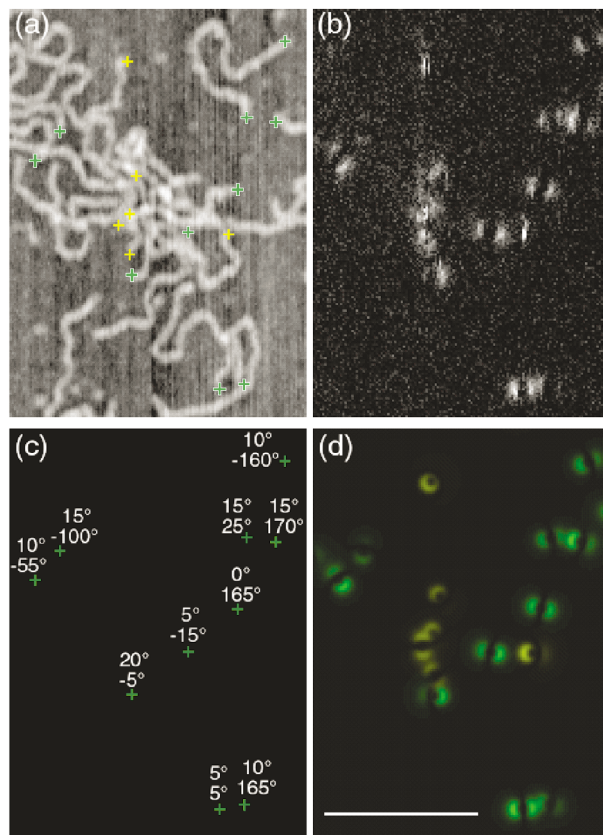


FIG. 5 (color). DNA with Cy-3 labeled termini on mica and corresponding data modeling. (a) Topography together with calculated positions of the analyzed dye molecules marked by “+.” (b) Fluorescence. (c) Positions as in (a), together with tilt angles (upper numbers) and azimuth angles (lower numbers) as resulting from our first approximation fits shown in (d). The fitted radius of the tip is 12 nm. Good fits are displayed in green; problematic fits due to, e.g., blinking or bleaching of the dyes are marked in yellow. The data in (a) are flattened (from each line, a fitted parabola has been subtracted). Scale bar: 200 nm.

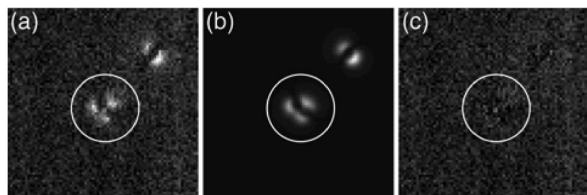


FIG. 6. Fluorescence pattern of two dyes located close to each other. (a) Experimental data. (b) Best fit when assuming two dyes for the encircled pattern, resulting distance 12 nm. (c) Difference between data (a) and fit (b). Outside the circle enclosing the pattern in question, a single dye molecule is visible. Image size: $300 \times 300 \text{ nm}^2$.

Figure 5 shows results of the optical measurements on the labeled DNA sample including the simultaneously taken topography, together with the results from the computer evaluation. As expected, most of the dye molecules are found at the termini of the DNA. In Fig. 5(a) and other measurements (not shown) about 60% of the detected dyes can clearly be assigned to a visible end of a DNA strand. The other dyes fall mostly into overcrowded regions where classification remains doubtful.

The positions of the dyes can be determined from the computational fits with high precision. Test calculations for various orientations and for noise parameters taken from Fig. 5 (background 61 c/pixel; standard deviation of the background 13 c/pixel; total counts per molecule: 7900) indicate an accuracy in the dye positions of 0.5 nm standard deviation. Within the validity of our simple model, the simultaneously determined azimuth angle is accurate to 5° and the accuracy of the tilt angle is better than 10° . Knowledge of the orientation of substructures is essential for many structural investigations. This orientation can be monitored by single dye molecules used as tags rigidly attached to the structures. Furthermore, the relative orientation of two dyes is an important parameter also in fluorescence resonance energy transfer distance measurements.

The two dyes at the right bottom of Fig. 5(b) with a distance of only 35 nm can easily be distinguished. Smaller distances with partly overlapping patterns can be resolved by computer-based analysis. The observed pattern shown in Fig. 6(a) can best be simulated by assuming two fluorophores in a distance of only 12 nm. Simulation by just one fluorophore fails to explain the observed pattern.

The presented results on imaging fluorescent-labeled single biomolecules demonstrate the enormous potential of our new SNOM approach. Its decisive advantage is the unique combination of several features: high-resolution optical signal at low background, simultaneous acquisition of an AFM-like topographical signal, single fluorophore sensitivity, access to the orientation of dyes, and accurate determination of their positions. Improvements of our probe are still to be expected by optimizing the tip-aperture geometry including variation of tip length and

material to allow plasmon resonances. Sharpening the metal tip will increase resolution as the apex radius seems to be the main limiting factor at moment. With the corresponding investigations the TOA method will contribute to a better understanding of field propagation along subwavelength sized metal structures and of field concentration at a sharp tip. Use of the presented new tool for imaging purposes promises exciting applications, especially in molecular and cellular biology.

The authors thank F. Keilmann, R. Hillenbrand, T. Taubner, and M. Stark for valuable discussions, M. Groves for critical reading and suggestions on the manuscript, and the Deutsche Forschungsgemeinschaft for financial support.

*Corresponding author.

Electronic address: guckenbe@biochem.mpg.de

- [1] For reviews, see B. Hecht *et al.*, *J. Chem. Phys.* **112**, 7761 (2000); H. F. Hamann, *Z. Phys. Chem.* **215**, 1025 (2001).
- [2] E. Betzig and R. J. Chichester, *Science* **262**, 1422 (1993).
- [3] N. F. van Hulst, J.-A. Veerman, M. F. García-Parajó, and L. Kuipers, *J. Chem. Phys.* **112**, 7799 (2000).
- [4] A. Naber *et al.*, *Phys. Rev. Lett.* **89**, 210801 (2002).
- [5] N. Hosaka and T. Saiki, *J. Microsc.* **202**, 362 (2001).
- [6] R. Eckert *et al.*, *Appl. Phys. Lett.* **77**, 3695 (2000). Here the probe was completely covered by a metal film.
- [7] S. Kawata and Y. Inouye, *Ultramicroscopy* **57**, 313 (1995).
- [8] R. Hillenbrand and F. Keilmann, *Appl. Phys. Lett.* **80**, 25 (2002).
- [9] J. Azoulay, A. Débarre, A. Richard, and P. Tchénio, *J. Microsc.* **194**, 486 (1999).
- [10] N. Hayazawa, Y. Inouye, and S. Kawata, *J. Microsc.* **194**, 472 (1999).
- [11] T. J. Yang, A. Guillaume, G. A. Lessard, and S. R. Quake, *Appl. Phys. Lett.* **76**, 378 (2000).
- [12] H. F. Hamann, A. Gallagher, and D. J. Nesbitt, *Appl. Phys. Lett.* **76**, 1953 (2000).
- [13] A. Kramer, W. Trabesinger, B. Hecht, and U. P. Wild, *Appl. Phys. Lett.* **80**, 1652 (2002).
- [14] W. Trabesinger *et al.*, *J. Microsc.* **209**, 249 (2003).
- [15] E. J. Sánchez, L. Novotny, and X. S. Xie, *Phys. Rev. Lett.* **82**, 4014 (1999).
- [16] H. G. Frey, F. Keilmann, A. Kriele, and R. Guckenberger, *Appl. Phys. Lett.* **81**, 5030 (2002).
- [17] B. Sick, B. Hecht, U. P. Wild, and L. Novotny, *J. Microsc.* **202**, 365 (2001).
- [18] C. W. Hollars and R. C. Dunn, *J. Chem. Phys.* **112**, 7822 (2000).
- [19] A. Bouhelier, M. Beversluis, A. Hartschuh, and L. Novotny, *Phys. Rev. Lett.* **90**, 013903 (2003).
- [20] R. R. Chance, A. Prock, and R. Silbey, *J. Chem. Phys.* **60**, 2744 (1974). Although this reference focuses on flat surfaces, Eq. (8) is generally valid independent of the geometry.
- [21] G. Cnossen, K. E. Drabe, and D. A. Wiersma, *J. Chem. Phys.* **98**, 5276 (1993).
- [22] H. Gersen *et al.*, *Phys. Rev. Lett.* **85**, 5312 (2000).